



Engineering and metrology of epitaxial graphene

Alexander Tzalenchuk^{a,*}, Samuel Lara-Avila^b, Karin Cedergren^b, Mikael Syväjärvi^c, Rositza Yakimova^c, Olga Kazakova^a, T.J.B.M. Janssen^a, Kasper Moth-Poulsen^d, Thomas Bjørnholm^e, Sergey Kopylov^f, Vladimir Fal'ko^f, Sergey Kubatkin^b

^a National Physical Laboratory, Teddington TW11 0LW, UK

^b Department of Microtechnology and Nanoscience, Chalmers University of Technology, S-412 96 Göteborg, Sweden

^c Department of Physics, Chemistry and Biology (IFM), Linköping University, S-581 83 Linköping, Sweden

^d College of Chemistry, University of California, Berkeley, 637 Latimer Hall, Berkeley, CA 94720, USA

^e Nano-Science Center & Department of Chemistry, University of Copenhagen, Universitetsparken 5, DK-2100, Denmark

^f Physics Department, Lancaster University, Lancaster LA1 4YB, UK

ARTICLE INFO

Article history:

Accepted 12 April 2011

by V. Fal'ko

Available online 23 June 2011

Keywords:

A. Graphene
D. Quantum Hall effect
D. Photochemical gate
E. Metrology

ABSTRACT

Here we review the concepts and technologies, in particular photochemical gating, which contributed to the recent progress in quantum Hall resistance metrology based on large scale epitaxial graphene on silicon carbide.

Crown Copyright © 2011 Published by Elsevier Ltd. All rights reserved.

1. Introduction

Graphene – a single layer of carbon atoms – is a truly two-dimensional gapless semiconductor with electrons mimicking the behaviour of relativistic (Dirac) electrons [1]. This feature of charge carriers in graphene is manifested most spectacularly through an unusual QHE [2]. The sequence of plateaux in the transverse resistance R_{xy} depends on the topological (Berry) phase acquired by the charge moving in the magnetic field. This phase is zero in conventional materials, where $R_{xy} = \pm \frac{h}{ne^2}$ ($n \geq 1$); it is equal to 2π in bilayer graphene [3,4] leading to a sequence of QHE plateaux at $R_{xy} = \pm \frac{h/4e^2}{n+1}$ ($n \geq 0$), and π in single-layer [5] with $R_{xy} = \pm \frac{h/4e^2}{n+1/2}$ ($n \geq 0$). The observation of this last sequence of QHE plateaux is therefore a smoking gun for the sample to contain monolayer graphene [2].

The quantum Hall effect [6] allows the international standard for resistance to be defined in terms of the electron charge and Planck's constant alone. The QHE resistance standard is believed to be accurate (no corrections to the fractions of $R_K = h/e^2$), universal (material-independent) and robust (same resistance over a range of magnetic field, temperature, current). However, only a

very small number of 2DEG structures – Si FET and group III–V heterostructures – satisfy these requirements. New materials are sought and graphene should in principle be an ideal material for an implementation of a quantum resistance standard, because of a very large spacing of the Landau levels compared to conventional 2DEGs [7].

In reality, an impressive range of unconventional transport properties of electrons in graphene [8], including QHE, had until recently been seen almost exclusively in flakes mechanically exfoliated from bulk graphite. Quantum Hall plateaux have been observed in graphene even at room temperature, albeit with an accuracy of 0.2% [9]. The highest experimentally achieved accuracy in exfoliated graphene flakes – 15 parts per million (ppm) at 300 mK [10] – is still modest by metrological standards. The main constraint appears to be the small area of the flakes, which limits the maximum non-dissipative current the system can sustain in the quantum Hall state. This is related both to high electrical resistance of the contacts and high thermal resistance of the graphene–substrate interface.

An alternative ‘top-down’ approach to produce graphene consists of growing it epitaxially. Epitaxial growth on SiC produces large area few-[11] or monolayer [12] graphene, however, initial attempts to observe QHE in such samples were unsuccessful. The difficulty was related to the lack of atomically accurate thickness control during the film growth on the C-terminated face of SiC, and

* Corresponding author.

E-mail address: alexander.tzalenchuk@npl.co.uk (A. Tzalenchuk).

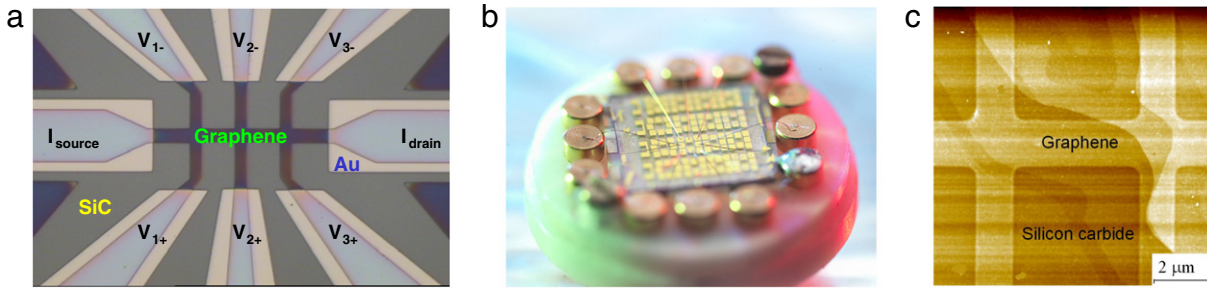


Fig. 1. (a) Optical micrograph of a Hall bar used in the experiments. (b) Layout of a $7 \times 7 \text{ mm}^2$ wafer with 20 Hall bars. (c) AFM image of a Hall bar. Meandering lines are steps in the substrate.

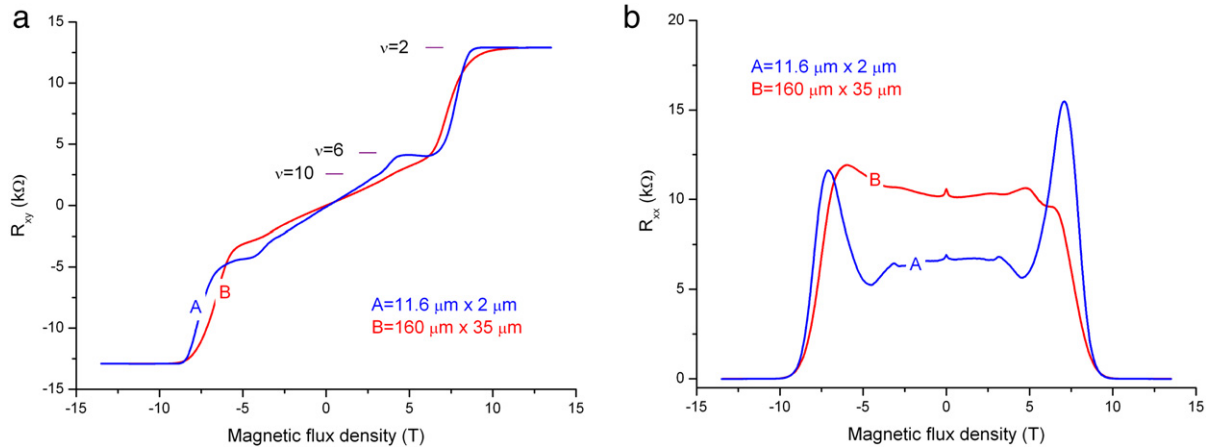


Fig. 2. Transverse (a) and longitudinal (b) resistance of a small and a large device measured at $T = 4.2 \text{ K}$ with $1 \mu\text{A}$ current.

most probably a strong variation of carrier density (doping) across the layers grown on the Si-terminated face [13]. A breakthrough came in 2009, when several groups within days of each other managed to produce epitaxial material of sufficient quality to demonstrate the QHE features typical of monolayer graphene [14–18]. In this paper we review our progress in engineering and precise magnetotransport measurements on epitaxial graphene devices that followed.

2. Precision resistance metrology on graphene

In [17] we reported the first metrologically precise measurements of the quantum Hall effect in a large high-quality epitaxial sample. The material studied in our experiments was grown on the Si-terminated face of a 4H-SiC(0001) substrate [19]. The reaction kinetics on the Si-face is slower than on the C-face because of the higher surface energy, which helps homogeneous and well-controlled graphene formation. Graphene was grown at 2000°C and 1 atm Ar gas pressure, which result in monolayers of graphene atomically uniform over more than $50 \mu\text{m}^2$, as shown by low-energy electron microscopy. Twenty Hall bar devices of different sizes, from $160 \mu\text{m} \times 35 \mu\text{m}$ down to $11.6 \mu\text{m} \times 2 \mu\text{m}$ were produced on each 0.5 cm^2 wafer using standard electron beam lithography and oxygen plasma etching (Fig. 1). Atomic force microscopy (AFM) images revealed that the graphene layer covers the substrate steps like a carpet, preserving its structural integrity. Contacts to graphene were produced by straightforward deposition of 3 nm of Ti and 100 nm of Au through a lithographically defined mask followed by lift-off, with the typical area of the graphene–metal interface of $10^4 \mu\text{m}^2$ for each contact. This process favourably compares with a laborious contact preparation to a two-dimensional electron gas in conventional semiconductor technology. Using low magnetic field measurements, we

established that the manufactured material was n-doped, with the measured electron concentration in the range of $(5\text{--}8) \times 10^{11} \text{ cm}^{-2}$, mobility about $2400 \text{ cm}^2/\text{V s}$ at room temperature and between 4000 and $7500 \text{ cm}^2/\text{V s}$ at 4.2 K, almost independent of device dimensions and orientation with respect to the substrate terraces.

Fig. 2 shows the longitudinal (dissipative) R_{xx} and the transverse (Hall) R_{xy} resistance of a $2 \mu\text{m}$ wide Hall bar at 4.2 K and magnetic field up to 14 T. At high magnetic field we clearly identified two QHE plateaux, at $R_{xy}^{(0)} = R_K/2$ ($n = 0$) and $R_{xy}^{(1)} = R_K/6$ ($n = 1$) corresponding to the filling factors $\nu = 2$ and $\nu = 6$ respectively. In graphene $\nu = 2$ corresponds to the fully occupied zero-energy Landau level ($n = 0$) characterised by the largest separation $\nu\sqrt{2\hbar eB/c}$ from other Landau levels in the spectrum and hence the Hall resistance quantisation is particularly robust. This plateau appeared in the field range of 9–12 T, depending on the carrier concentration (which was beyond our control in those experiments) and was accompanied by a vanishing R_{xx} . The $n = 1$ plateau, at $\nu = 6$, was not so flat, and R_{xx} developed only a weak minimum. There was also a trace of a structure corresponding to $\nu = 10$. The observed sequence of Hall plateaux confirmed that the studied material was indeed monolayer graphene. At low magnetic fields we observed Shubnikov–de Haas oscillations as well as a weak localisation peak characteristic of the phase coherence of electrons in a disordered conductor.

The magneto-transport measurements on a much bigger, $160 \mu\text{m} \times 35 \mu\text{m}$ Hall bar device are also presented in Fig. 2. A substantial positive magnetoresistance at low fields, which was absent in the smaller sample, indicated that the carrier concentration varied along the larger sample. Because of that, the $\nu = 6$ feature in R_{xx} in the bigger sample was less prominent. Nevertheless, despite the inhomogeneity of the carrier density, the Hall resistance plateau at $R_{xy}^{(0)} = R_K/2$ ($n = 0$) was accompanied

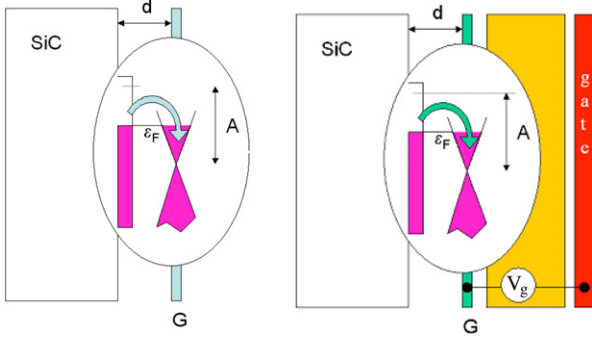


Fig. 3. Charge transfer between SiC and bare/gated graphene.

by vanishing longitudinal resistance R_{xx} . Importantly, the large-area device had a low resistance $R_c \approx 1.5 \Omega$ of contacts to the graphene layer and, as compared to smaller devices, could sustain a much higher current before QHE breaks down. We have found that contacts made with Pd yielded even lower contact resistance down to 0.6Ω . Since larger breakdown current affords higher precision measurements in the QHE regime, we chose to perform such measurements in the larger sample. The choice of the field, 14 T, where the most accurate measurements were performed was determined simply by the limitation of our superconducting magnet. This limit is below $B = 17.5$ T where the filling factor would be exactly $\nu = 2$ for this sample (with $n_s = 8.5 \times 10^{11} \text{ cm}^{-2}$ calculated from SdH oscillations).

The accuracy of Hall resistance quantisation in graphene was established in measurements traceable to the GaAs quantum Hall resistance standard using a calibrated 100Ω resistor. The optimal conditions at 300 mK were obtained for a source–drain current of $11.6 \mu\text{A}$, 15% below the breakdown current established in the measurements of R_{xx} . The quantisation accuracy $+0.4 \pm 3$ parts in 10^9 inferred from our measurements was a four orders of magnitude improvement on the previous best result in exfoliated graphene. Graphene was still accurately quantised at 4.2 K, however, at this temperature the measurement current had to be reduced to $2.3 \mu\text{A}$, which increased the uncertainty of the data accumulated over a comparable time interval.

The reported result readily put epitaxial graphene quantum Hall devices in the same league as their semiconductor counterparts. Note that it was obtained on a sample, although large by graphene standards, substantially smaller than the semiconductor devices used for calibration and without any optimisation. The precision measurements were made as far inside the resistance plateau as our magnet could reach, but still a long way from $\nu \equiv 2$. Further progress demanded the ability to engineer the carrier density and control the uniformity of charge distribution in epitaxial graphene.

3. Constraints on the tunability of the carrier density in epitaxial graphene

Before embarking in a technological quest to control the carrier density, we should explain why the epitaxial graphene is always strongly n-doped and what constraints does it impose on the tunability of the carrier density. In [20] we presented a theoretical model of charge transfer from the SiC substrate to monolayer or bilayer graphene at zero magnetic field.

The charge transfer [21] between bulk/surface donors under/on SiC surface onto graphene (Fig. 3) can be written as

$$\begin{cases} \gamma[A - 4\pi d e^2 n - \varepsilon_F] + \rho l = n, \\ \tilde{A} = \varepsilon_F + U + 4\pi d e^2 n. \end{cases} \quad (1)$$

The first of these two equations expresses the charge balance. Here $\varepsilon_F = v\hbar\sqrt{\pi n}$ is the Fermi level in graphene formed upon charge transfer, $v = 10^8 \text{ cm/s}$ is the Dirac velocity of electrons in graphene, $A(\tilde{A})$ are the differences between the work function for electrons in un-doped graphene and surface (bulk) donor states in SiC, ρ is the volume density of donors in SiC, which are depleted to the depth l , and γ is the density of states (DoS) of the surface states. The distance d between graphene and the SiC surface, and the Schottky barrier $U = (2\pi e^2/\chi)\rho l^2$ (with $\chi \sim 10$) formed inside SiC determine the thermal equilibrium between electrons in graphene and donors, the second line in Eq. (1). For an electrostatically gated device the charge is distributed between graphene and the gate, so we need to substitute n by $(n+n_g)$ in Eq. (1), where the gate charge $n_g = CV_g/e$ is determined by the gate-to-graphene capacitance C and voltage V_g . The analysis [20] of Eq. (1) shows that graphene in SiC with either $\gamma > \gamma_* = \frac{4A}{\pi\hbar^2 v^2} (1 + \sqrt{1 + \frac{16Ade^2}{\hbar^2 v^2}})^{-2}$ or $\rho > \rho_* = \frac{32\tilde{A}^3 e^2}{\pi\chi\hbar^4 v^4} (1 + \sqrt{1 + \frac{16Ade^2}{\hbar^2 v^2}})^{-4}$ acquires the initial electron density

$$n_* = \frac{4A_m^2}{\pi\hbar^2 v^2} \left(1 + \sqrt{1 + \frac{16A_m d e^2}{\hbar^2 v^2}} \right)^{-2}, \quad (2a)$$

where $A_m = \tilde{A}$ if $\gamma < \gamma_*$ and $\rho > \rho_*$, $A_m = A$ if $\gamma > \gamma_*$ and $\rho < \rho_*$, and $A_m = \max\{A, \tilde{A}\}$ if $\gamma > \gamma_*$ and $\rho > \rho_*$. This density is then difficult to change using gates. For a less doped SiC, with both $\gamma < \gamma_*$ and $\rho < \rho_*$, the charge transfer onto graphene can be less than the limiting value n_* ,

$$n = \max \left\{ \sqrt{\frac{\tilde{A}\chi}{2\pi e^2}} \rho; A\gamma \right\} \quad (2b)$$

and it can be then efficiently varied using electrostatic gates. Having estimated the limiting electron density in graphene for $A_m \sim 1 \text{ eV}$ and $d \sim 0.3 \text{ nm}$ we arrive at $n_* \approx 10^{13} \text{ cm}^{-2}$, which is close to the typical density of graphene doping observed in many recent studies of epitaxial graphene [12,14,22,23].

The above consideration suggests that the reduction of donors on or just under the SiC surface is crucial for the use of epitaxial graphene on SiC in gated devices. We note that our graphene samples were grown at $2000 \text{ }^\circ\text{C}$ – a substantially higher temperature than in other published reports. These conditions reliably produced a carrier density of $n \sim 10^{12} \text{ cm}^{-2}$ much lower than n_* . We speculate that high-temperature annealing of SiC compensates surface donor states, possibly through surface segregation of impurities (e.g., B or N) abundant in bulk SiC crystals, or merely reduction of the number of surface defects.

4. Controlling the charge carrier density in epitaxial graphene

Methods for precise control of the carrier density in electronic materials are the cornerstones of the modern semiconductor technology. Chemical methods ranging from direct doping to modulation doping have been developed to absolute perfection for semiconductors over the last half-century. Graphene can also be effectively doped for example by adsorption of gas molecules [24]. In addition to permanent doping, the electronic properties of semiconductor materials and graphene can be changed by the electric field produced by a charged gate, as in a transistor, but this requires an external voltage source permanently connected to maintain the stored charge. Semiconductor programmable nonvolatile memory devices give us an inspirational example of how the carrier density of materials can be changed, latched and then erased. These devices are essentially transistors with one

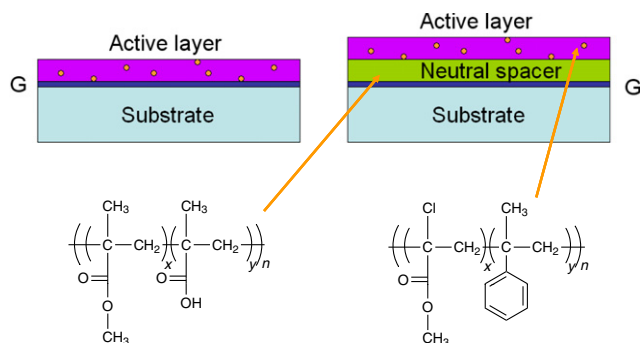


Fig. 4. In direct chemical gating electrons in graphene can scatter on the ions in the adjacent active layer. When graphene is encapsulated in a polymer bilayer the active polymer (ZEP) is separated from graphene by a neutral spacer (COP).

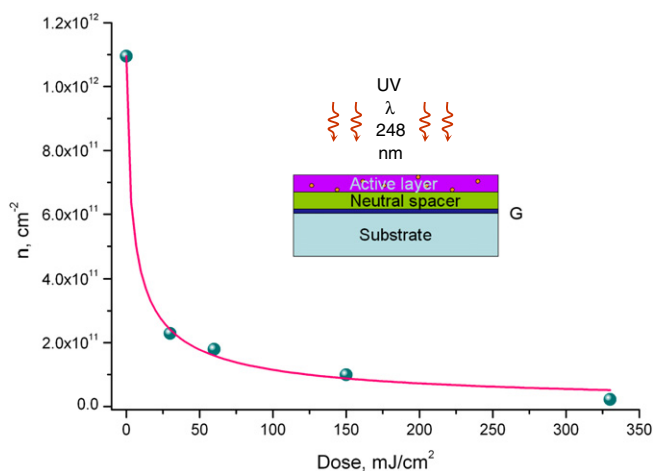


Fig. 5. Photochemical gating of graphene.

extra floating, isolated gate sandwiched between the control gate and the semiconductor channel. Charge can be transferred to the floating gate by an electric pulse on the control gate and stored there isolated almost infinitely, until intentionally leaked through the dielectric, e.g. activated by UV light. In other implementations of the nonvolatile memory devices UV light is used for writing [25,26] in which case thermal activation can be used for erasing.

Though, unsurprisingly, a relatively low density in the epitaxial graphene grown with the technology [19] briefly summarised above could be further reduced by applying voltage between a metallic gate and graphene across a PMMA/MMA copolymer (COP) spacer, methods of non-invasive, nonvolatile and reversible charge carrier control would be particularly important for the engineering of devices for metrology, where we would rather avoid an additional electrically controlled parameter, which brings additional noise.

To achieve the nonvolatile control of the carrier density we replaced the metal gate with another polymer layer – ZEP520A, hereafter ZEP, chosen for its ability to provide potent acceptors under deep UV light, and demonstrated **photochemical gating** [27] of graphene (see the layout of the heterostructure and the chemical formulae of the polymers in Fig. 4). In a sample with the initial carrier density $n \approx 1.1 \times 10^{12} \text{ cm}^{-2}$, subsequent exposures to UV at 248 nm wavelength up to the dose of 330 mJ/cm^2 decreased the low-temperature electron density 50 times down to $2 \times 10^{10} \text{ cm}^{-2}$ (Fig. 5). This resulted in a fivefold increase in carrier mobility up to 16000 $\text{cm}^2/\text{V s}$ at the liquid helium temperature and a tenfold increase in resistivity of graphene. The irradiated devices remained latched in their high-resistivity state

over many months. The “on/off” ratio of 10 for the resistivity of the photochemically-gated devices is similar to the best large-area single-layer graphene transistors demonstrated to date [28]. Very significantly, annealing the samples at 170 °C – just above the glass transition temperature of the polymers – reversed the effects of light and returned the graphene charge carrier density to its value prior to UV exposure. The behaviour measured at room temperature was qualitatively the same as the one observed at low temperatures. In particular, the room temperature mobility has increased to 5130 $\text{cm}^2/\text{V s}$.

The mechanism of photochemical gating is different from the direct chemical doping [14,29,30], where the dopants are sitting on top of graphene. One has to consider the photochemistry of the polymers to understand the choice of the active layer and explain the light-induced effects. It is generally accepted that both COP and ZEP polymers undergo a photo-induced scission type reaction when exposed to an electron beam or UV light [31,32]. The mechanism for the ZEP polymer predominantly proceed via an initial homolytic bond cleavage of the C–Cl bond into a neutral Cl-radical and a neutral carbon radical [33]. The result is formation of a photo-induced abundance of Cl-radicals that are potent electron acceptors. Since COP does not possess any Cl, this mechanism cannot take place. In a control experiment, the graphene sample protected with only 330 nm of COP and no ZEP was exposed to UV light with a dose of 30 mJ/cm^2 and the result was a mere 1.5 times increase in the electron density, confirming that ZEP is the layer responsible for providing electron acceptors and suggesting that a small number of levels produced by the UV exposure in COP are working effectively as electron donors.

5. Quantum Hall effect in graphene/polymer heterostructures

In order to establish the sample quality resulting from encapsulation, we performed measurements at 4.2 K on the same large sample, which had been already thoroughly investigated in its pristine form. Results are summarised in Fig. 6. The red lines show longitudinal and transverse resistances, R_{xx} and R_{yy} , of the original bare sample with the carrier density of $1.1 \times 10^{12} \text{ cm}^{-2}$ and carrier mobility 2640 $\text{cm}^2 \text{ V}^{-1} \text{ s}^{-1}$ determined from the low-field magnetotransport measurements. Blue lines are the same for the encapsulated sample with $n = 7.8 \times 10^{11} \text{ cm}^{-2}$ and $\mu = 6340 \text{ cm}^2 \text{ V}^{-1} \text{ s}^{-1}$. When untreated, despite providing record quantisation accuracy of 3 parts in a billion, this very large sample had revealed spatial inhomogeneities not observed on a smaller scale (cf. 2 μm sample). The encapsulated sample revealed a flat R_{xx} background near zero field in place of a parabolic background in the untreated sample, significantly enhanced Shubnikov–de Haas oscillations of R_{xx} , sharper quantum Hall plateaux corresponding to $\nu = 6$ and also a visible trace of structures corresponding to $\nu = 10$ – the sequence characteristic of single layer graphene. Taken together these data show that encapsulation resulted in a significantly more uniform distribution of charge density in the sample.

Better quality and stability of the sample achieved by encapsulation and a reduced carrier density as a result of photochemical gating allowed metrological measurements with even higher precision than before. In particular as seen in Fig. 7 the breakdown current has increased from 13.3 to 35 μA . The longitudinal resistance is now very accurately zero and the Hall plateau extends over more than a tesla (Fig. 8). This is a manifestation of robustness of QHE achieved through encapsulation. It facilitated even more precise quantum Hall resistance measurements to be performed and we have demonstrated a precision of 0.3 ppb – an order of magnitude better than had been reported on the bare, uncoated sample.

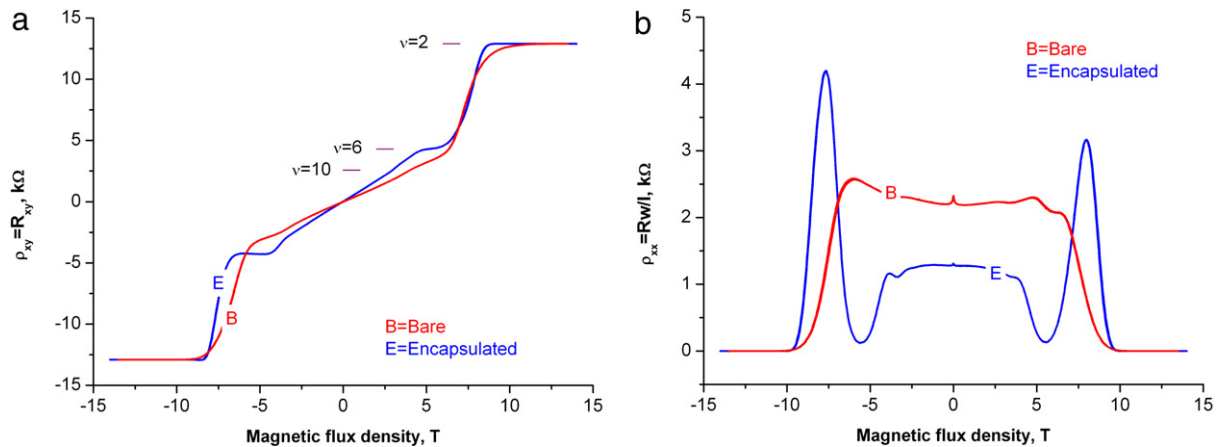


Fig. 6. Transverse (a) and longitudinal (b) resistance of the large $160 \mu\text{m} \times 35 \mu\text{m}$ device as in Fig. 2 before and after encapsulation.

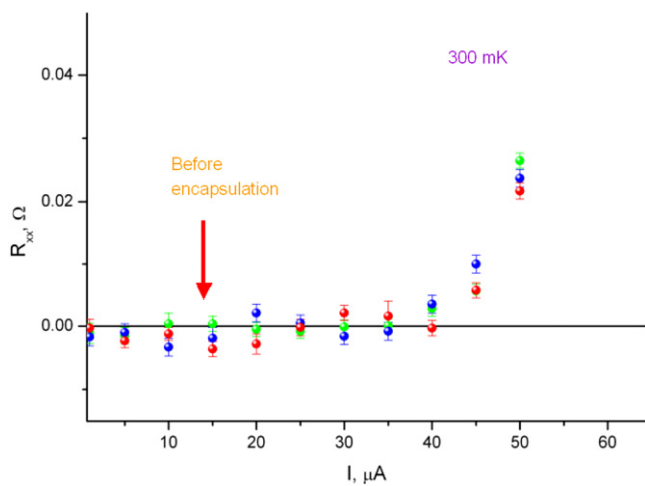


Fig. 7. Determination of the breakdown current of an encapsulated sample. The arrow shows the value before encapsulation.

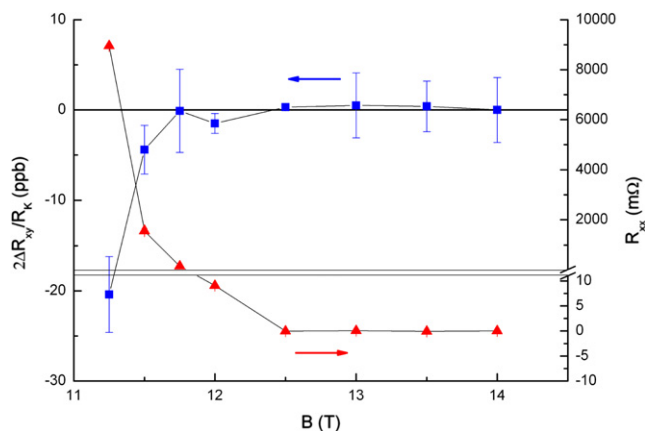


Fig. 8. Precision measurement of the transverse and longitudinal resistance of the encapsulated sample.

6. Conclusion

A significant progress has been achieved in graphene quantum Hall metrology in a few previous years. Graphene has passed the quantum Hall effect test – the benchmark of the maturity of the 2DEG technology in all its complexity including growth, patterning, ability to fabricate low-ohmic contacts and control the carrier density across the sample. Future development will include

investigation of the dissipation mechanisms in the quantum Hall regime, direct comparison of quantisation in graphene against GaAs and development of graphene quantum Hall arrays.

The photochemical gating technique may find a variety of applications far beyond metrology. To improve the on/off ratio of the SiC/G/polymer devices, one may use bilayer graphene [3] (BLG). Despite the challenges of developing the growth protocol for the BLG synthesis on SiC with a low initial carrier doping [34], BLG has a great advantage determined by its peculiar spectrum: a transverse electric field opens an interlayer asymmetry gap for electrons in BLG [3,34–36]. In optically gated SiC/G/polymer structures driven to the low carrier density by UV exposure, such a field naturally appears due to the layers of positive donor charge on SiC surface and the electron charge transferred to acceptors in ZEP. For structures with initial density $n \sim 10^{12} \text{ cm}^{-2}$, such a gap in a device driven to the neutrality point by photo-chemical gating can be estimated [37] as $\Delta \sim 10 \text{ meV}$, which is sufficiently high to modulate the room temperature conductivity [38].

More generally, this side of the work is connecting the young and rapidly developing field of graphene electronics and the mature field of organic electronics. We foresee practical devices like hybrid graphene/polymer sensors, where the polymer can be sensibilised to respond to a specific stimulus leading to a change in the conductance of the underlying graphene.

The quantum Hall effect proves that graphene retains its unique 2D properties when embedded in polymer heterostructures despite their complex architecture and maintains its characteristics over a long time. Metrology of graphene and graphene heterostructures is instrumental in providing confidence in future applications of this remarkable material.

References

- [1] K.S. Novoselov, A.K. Geim, S.V. Morozov, D. Jiang, M.I. Katsnelson, I.V. Grigorieva, S.V. Dubonos, A.A. Firsov, *Nature* 438 (7065) (2005) 197–200.
- [2] Y.B. Zhang, Y.W. Tan, H.L. Stormer, P. Kim, *Nature* 438 (7065) (2005) 201–204.
- [3] E. McCann, V.I. Fal'ko, *Phys. Rev. Lett.* 96 (8) (2006) 086805.
- [4] K.S. Novoselov, E. McCann, S.V. Morozov, V.I. Fal'ko, M.I. Katsnelson, U. Zeitler, D. Jiang, F. Schedin, A.K. Geim, *Nat. Phys.* 2 (3) (2006) 177–180.
- [5] A.H. Castro, F. Neto, N.M. Guinea, R. Peres, K.S. Novoselov, A.K. Geim, *Rev. Mod. Phys.* 81 (1) (2009) 109–162.
- [6] K.v. Klitzing, G. Dorda, M. Pepper, *Phys. Rev. Lett.* 45 (6) (1980) 494.
- [7] W. Poirier, F. Schopfer, *Eur. Phys. J. - Spec. Top* 172 (2009) 207–245.
- [8] A.K. Geim, *Science* 324 (5934) (2009) 1530–1534.
- [9] K.S. Novoselov, Z. Jiang, Y. Zhang, S.V. Morozov, H.L. Stormer, U. Zeitler, J.C. Maan, G.S. Boebinger, P. Kim, A.K. Geim, *Science* 315 (5817) (2007) 1379.
- [10] A.J.M. Giesbers, G. Rietveld, E. Houtzager, U. Zeitler, R. Yang, K.S. Novoselov, A.K. Geim, J.C. Maan, *Appl. Phys. Lett.* 93 (22) (2008) 222109.
- [11] C. Berger, Z.M. Song, T.B. Li, X.B. Li, A.Y. Ogbazghi, R. Feng, Z.T. Dai, A.N. Marchenkov, E.H. Conrad, P.N. First, W.A. de Heer, *J. Phys. Chem. B* 108 (52) (2004) 19912–19916.

- [12] K.V. Emtsev, A. Bostwick, K. Horn, J. Jobst, G.L. Kellogg, L. Ley, J.L. McChesney, T. Ohta, S.A. Reshanov, J. Rohrl, E. Rotenberg, A.K. Schmid, D. Waldmann, H.B. Weber, T. Seyller, *Nat. Mater.* 8 (3) (2009) 203–207.
- [13] P. Darancet, N. Wipf, C. Berger, W.A. de Heer, D. Mayou, *Phys. Rev. Lett.* 101 (11) (2008) 116806.
- [14] J. Jobst, D. Waldmann, F. Speck, R. Hirner, D.K. Maude, T. Seyller, H.B. Weber, *Phys. Rev. B* 81 (19) (2010) 195434.
- [15] T. Shen, J.J. Gu, M. Xu, Y.Q. Wu, M.L. Bolen, M.A. Capano, L.W. Engel, P.D. Ye, *Appl. Phys. Lett.* 95 (17) (2009) 172105.
- [16] S. Tanabe, Y. Sekine, H. Kageshima, M. Nagase, H. Hibino, *Appl. Phys. Express* 3 (7) (2010) 075102.
- [17] A. Tzalenchuk, S. Lara-Avila, A. Kalaboukhov, S. Paolillo, M. Syvajarvi, R. Yakimova, O. Kazakova, T.J.B.M. Janssen, V. Fal'ko, S. Kubatkin, *Nat. Nanotechnol.* 5 (3) (2010) 186–189.
- [18] X.S. Wu, Y.K. Hu, M. Ruan, N.K. Madiomanana, J. Hankinson, M. Sprinkle, C. Berger, W.A. de Heer, *Appl. Phys. Lett.* 95 (22) (2009) 223108.
- [19] C. Virojanadara, M. Syvajarvi, R. Yakimova, L.I. Johansson, A.A. Zakharov, T. Balasubramanian, *Phys. Rev. B* 78 (24) (2008) 245403.
- [20] S. Kopylov, A. Tzalenchuk, S. Kubatkin, V.I. Fal'ko, *Appl. Phys. Lett.* 97 (11) (2010) 112109.
- [21] J. Bardeen, *Phys. Rev.* 71 (10) (1947) 717–727.
- [22] C. Coletti, C. Riedl, D.S. Lee, B. Krauss, L. Patthey, K. von Klitzing, J.H. Smet, U. Starke, *Phys. Rev. B* 81 (23) (2010) 235401.
- [23] J.S. Moon, D. Curtis, S. Bui, M. Hu, D.K. Gaskill, J.L. Tedesco, P. Asbeck, G.G. Jernigan, B.L. VanMil, R.L. Myers-Ward, C.R. Eddy, P.M. Campbell, X. Weng, *IEEE Electr. Device L* 31 (4) (2010) 260–262.
- [24] T.O. Wehling, K.S. Novoselov, S.V. Morozov, E.E. Vdovin, M.I. Katsnelson, A.K. Geim, A.I. Lichtenstein, *Nano. Lett.* 8 (1) (2008) 173–177.
- [25] L.A. Glasser, in: H. Fuchs (Ed.), *Chapel Hill Conference on VLSI*, Computer Science Press, Rockville, MD, 1985, pp. 61–65.
- [26] D.A. Kerns, J. Tanner, M. Sivillotti, J. Luo, in: C.H. Sequin (Ed.), *Advanced Research in VLSI*, MIT Press, Cambridge, MA, 1991, pp. 245–261.
- [27] S. Lara-Avila, K. Moth-Poulsen, R. Yakimova, T. Bjornholm, V. Fal'ko, A. Tzalenchuk, S. Kubatkin, *Adv. Mater.* 23 (7) (2011) 878–882.
- [28] F. Schwier, *Nat. Nanotechnol.* 5 (7) (2010) 487–496.
- [29] K. Brenner, R. Murali, *Appl. Phys. Lett.* 96 (6) (2010) 063104.
- [30] T. Lohmann, K. von Klitzing, J.H. Smet, *Nano. Lett.* 9 (5) (2009) 1973–1979.
- [31] T. Nishida, M. Notomi, R. Iga, T. Tamamura, *Jpn. J. Appl. Phys.* 1 31 (12B) (1992) 4508–4514.
- [32] K.K. Okudaira, E. Morikawa, S. Hasegawa, P.T. Sprunger, V. Saile, K. Seki, Y. Harada, N. Ueno, *J. Electron Spectrosc.* 88 (1998) 913–917.
- [33] H. Ikeura-Sekiguchi, T. Sekiguchi, M. Koike, *J. Electron Spectrosc.* 144 (2005) 453–455.
- [34] T. Ohta, A. Bostwick, T. Seyller, K. Horn, E. Rotenberg, *Science* 313 (5789) (2006) 951–954.
- [35] J.B. Oostinga, H.B. Heersche, X.L. Liu, A.F. Morpurgo, L.M.K. Vandersypen, *Nat. Mater.* 7 (2) (2008) 151–157.
- [36] Y.B. Zhang, T.T. Tang, C. Girit, Z. Hao, M.C. Martin, A. Zettl, M.F. Crommie, Y.R. Shen, F. Wang, *Nature* 459 (7248) (2009) 820–823.
- [37] E. McCann, *Phys. Rev. B* 74 (16) (2006) 161403.
- [38] B.N. Szafranek, D. Schall, M. Otto, D. Neumaier, H. Kurz, *Appl. Phys. Lett.* 96 (11) (2010) 112103.